CELLULAR DECISION MAKING AT THE NANOSCALE

BY

ZAINAB RAHIL

THESIS

Submitted in partial fulfillment of the requirements
for the degree of Master of Science in Bioengineering
in the Graduate College of the
University of Illinois at Urbana-Champaign, 2016

Urbana, Illinois

Advisors:

Professor Deborah Leckband

Professor Taekjip Ha

ABSTRACT

The well-established dependence of cell traction forces on the compliance of supporting matrices has been attributed to levels of force exerted on components in focal contacts. Here, use of novel, force-limited nanoscale tension gauges revealed that both force and substrate deformations govern cell decision-making during initial attachment to compliant substrates. We propose a mechanical model consistent with observed behavior. Upon formation of stable cell contacts, bond tension and tether rupture govern cell attachment, spreading, and focal adhesion maturation at force levels on individual receptors predicted by prior studies.

ACKNOWLEDGEMENTS

I would like to acknowledge my advisors Dr. Leckband and Dr. Ha. Along with them I would like to acknowledge Dr. Harley and Dr. Pedron. I would also like to acknowledge all the members of Leckband lab.

I would like to acknowledge my parents, Rahil Mohammad Khan and Rabia Rahil, my dadi, Aziza Khanum, my siblings Mahrukh, Hussein, Jahanzeb, Sara, Sohaib and my nephew, Abbas, for their constant love and support. Lastly I would like to acknowledge all my friends here in Champaign- particularly Ahmad, Zain, Shayan, Tooba, Mariyam, Anum H., Anum J., and Asim for being family away from family.

TABLE OF CONTENTS

INTRODUCTION

It is well established that cells sense substrate rigidity through integrin-based focal adhesions (FA) to extracellular matrix (ECM) proteins to regulate cell attachment, spreading, and focal adhesion maturation on compliant materials [1-4]. Studies of cell spreading on nanopatterned and deformable substrates or micropillar arrays revealed cellular decision-making at different stages of spreading that was instructed by different biophysical triggers [5-8]. The molecular origins of those biophysical cues, the forces involved, and their dependence on substrate rigidity are still subjects of intensive investigation, motivated in part by evidence that the underlying molecular events contribute to stem cell lineage specification and disease [9-13].

Diverse studies revealed molecular and cellular processes that govern cell behavior at different stages of adhesion and spreading on soft versus rigid substrates. Initial ligation is sufficient to activate integrin clustering, without force application[14]. Studies suggested that tension generated by integrin-actomyosin engagement switches integrin-ligand cross-links to a higher affinity, signaling-competent state that activates FA maturation [14]. Substrate mechanics appears to alter the transition to the tensioned state [4]; AFM data suggested that integrin-ligand bonds are weaker in cells on soft versus rigid substrates. Similarly, α5β1 integrin reportedly formed fewer, high affinity cross-links to ECM on softer gels [14]. Stem cells on soft surfaces also exhibited greater α5 integrin activation relative to cells on rigid ECM, and the former coincided with greater integrin internalization [9].

Cell adhesion and spreading following initial integrin ligation is further postulated to occur in three phases governed by membrane tension and forces exerted on focal contacts [5, 7]. In the initial attachment phase, P0, ligation activates integrins, but if there is insufficient tension to activate cell spreading, then cells remain rounded [14, 15]. Tension on focal contacts activates the cell-spreading transition. An identified early phase of cell spreading (P1) involves rapid, circumferential extension of lamellipodia with only weak cell contractions [7]. The extension of excess membrane increases membrane tension [5].

Upon reaching about 60% of the final spread area, myosin II activated contractions signal the transition to the contractile phase P2, which is characterized by periodic contractions, postulated rigidity sensing, and focal adhesion (FA) maturation. In some cases, the forces that actuate these changes were estimated using optical tweezers or measured changes in membrane tension [5, 16]. However, determining the forces that activate cellular behavior typically involves external perturbations, and biophysical approaches often lack the sensitivity to quantify relevant cellular or molecular forces.

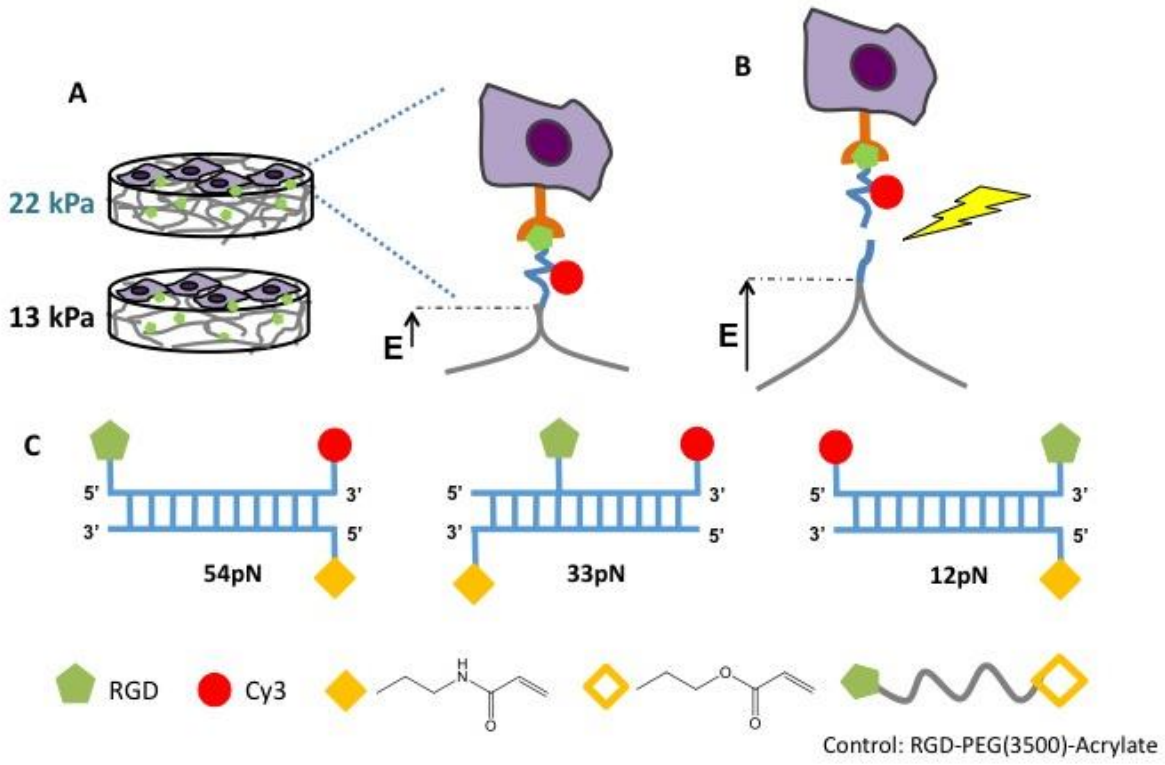

Figure 1. Schematic of the force response of TGTs on soft substrates. **(A)** Cell attachment to TGT modified hydrogels with elastic moduli of 13kPa (soft) and 22kPa (rigid). **(B)** Cells deform the substrates until the tension exceeds T_{tol} and the cells tear off the sensing strand (yellow jagged arrow). **(C)** DNA duplex tethers with tunable tension tolerance T_{tol}. The anchor DNA is covalently linked to the gel through polymerizable monomers (yellow triangles). The 'reporter' strand contains a 3' Cy3 dye (red circle) and the location of the RGD peptide along the strand (green pentagon) determines

The development of diverse autonomous, non invasive force reporters has enabled nanoscale in situ measurements of forces on mechanically stressed adhesion molecules [17-22]. Of the various molecular force sensors, Tension Gauge Tethers (TGTs) are novel force reporters that are based on a double stranded DNA backbone, in which the reporter strand is modified with an adhesion ligand and a fluorescent dye Cy3 (Fig. 1C) [22]. If force exerted on the TGT exceeds the tension tolerance of the tether, cells tear the reporter strand off the substrate (Fig. 1B). The ligand position along the reporter strand determines the force threshold to rupture the dsDNA, or the tension tolerance, T_{tol}, which can be tuned from ~12pN to >100pN (Fig. 1C). The TGTs increase the dynamic range beyond, for example, force sensors based on spider silk protein [20]. When anchored to substrates, TGTs cap the bond tension, and TGT rupture reports the force exerted on individual adhesive contacts. The Cy3 reporter can also be imaged at the single molecule level.

This study used RGD-modified TGTs to investigate threshold forces on individual integrin-ligand bonds required to support cell attachment, and to initiate transitions activating cell spreading and focal adhesion maturation on soft and rigid hydrogel substrates. The TGTs reported pico Newton forces exerted on individual integrin bonds that support initial, stable cell attachment, as well as indicate force thresholds that instruct subsequent cell spreading transitions. Importantly, differences in cell attachment densities on soft and rigid surfaces modified with identical tension gauges revealed novel coupling between substrate rigidity and bond tension. The observed differences in force thresholds on soft versus rigid substrates could not be attributed to bond force alone. Here, we propose a phenomenological mechanical model that predicts how substrate deformations and bond rupture forces coordinately modulate tension thresholds that guide cellular behavior in different mechanical environments.

MATERIALS AND METHODS

1. TGT synthesis.

Integrin-binding TGTs were generated, by conjugating cyclic peptide RGDfK to one DNA strand of a rupturable dsDNA tether. The other strand of the dsDNA was labeled with an acrydite tag at a desired position, for tethering to the hydrogel (Fig. 1C). The position of the RGDfK on the dsDNA determines tension at which the tethers rupture. The complementary ssDNA was acrydite-labeled 5-Acrydite/GGC CCG CAG CGA CCA CCC-3. The ssDNAs were purchased from Integrated DNA technologies, Inc. The tension tolerance is determined by the position of the reactive ThioMC3 and fluorescent Cy3 label in the nucleic acid sequence. The ThioMC3 positions in different TGTs with the indicated tension tolerance are given below:

54 pN TGT: 5-/5ThioMC3-D/ GGG TGG TCG CTG CGG GCC /Cy3/-3
33 pN TGT: 5-/5Cy3/GGGTGGTCGCT/iThioMC6-D/GCGGGCC/-3
12 pN TGT: 5-/5Cy3/GGGTGGTCGCTGCGGGCC/3ThioMC3-D/ -3

The cyclic peptide RGDfK-NH2 (catalog #: PCI-3696-PI) from Peptides International, Inc. RGDfK was conjugated to ThioMC3 on ssDNA using the hetero-bifunctional crosslinker Sulfo-SMCC (22622, Thermo Fisher Scientific Inc.), which has reactive maleimide and NHS ester groups on the two ends. The maleimide reacted with the thiol-modified DNA and the NHS covalently coupled to the N-terminal amine on RGDfK. The RGDfK-DNA and acrydite-DNA were then annealed in ‘annealing buffer’ (150mM NaCl, 10mM Tris, PH 7.4) at room temperature. In Phosphate Buffered Saline (PBS) at pH 7.4, the melting temperature of the dsDNA tethers is 73 °C.

The control, non rupturable tether was prepared by reacting a 3500 MW Acrylate PEG-NHS ester (JenKem Technology USA, Allen, TX) with RGDfK-NH2 at a molar ratio of 24:1 (PEG-NHS: RGD-NH_2), at room temperature in PBS at pH 8.0. Unreacted PEG-NHS was removed, using a 10K MW Pierce Concentrator PES (Thermo Scientific, Waltham, MA).

2. Hydrogel preparation and characterization.

To generate hydrogels with different Young's moduli, 7.5kDa PEG diacrylate macromers (Jenkem Technology) were mixed at 7 and 10 wt% in PBS, containing the TGT and 0.1% (w/v) lithium phenyl-2,4,6-trimethylbenzoylphosphinate (LAP) as a photoinitiator (Fairbanks and Anseth, Biomaterials 2009, 30, 6702). The double ring structure of Cy3 sterically hinders reactivity of methacrylamide groups in the 54 pN probes, during photo polymerization with PEG-diacrylate. Therefore, the initial tether concentration was adjusted in the prepolymer solution to achieve 1.5 μM of covalently bonded RGD for all samples. The initial TGT concentrations were 1.5 μM (12pN), 1.2 μM (33pN) and 2.2 μM (54pN). The prepolymer solution was then pipetted into 1 mm thick, circular Teflon molds of 5 mm diameter and exposed to 10 mW/cm^2 UV light (365 nm) for 90s at room temperature. The hydrogel disks were then detached from the mold and washed.

Mechanical analyses of the resulting hydrogels were performed on water swollen hydrogel disks, at room temperature via an MTS Insight mechanical testing apparatus at a rate of 20% strain/min. The compressive modulus was determined from the linear region corresponding to 0-5% strain. The relative tether concentrations bound to the hydrogels were determined from Cy3 fluorescence measurements. The fluorescence intensity was quantified before and after washing, and different preparations were compared to assess the relative amounts of covalently bound TGTs on each of the hydrogels (Fig. S1). Imaging was performed using a Zeiss LSM 710 NLO laser scanning confocal microscope (Carl Zeiss, Thornwood, NY, USA).

3. Cell culture and analyses.

Cells were seeded on 8 different substrates with elastic moduli of 13 and 22 kPa that were surface modified with RGD-functionalized TGTs with tension tolerances of 12, 33, or 54 pN. The non rupturable PEG-RGD was used as the control for both substrates. These tether forces were selected according to previously published data that shows a cells adhesion threshold at 40 pN. B16F1, CHOK1 and U87MG cell lines (from ATCC) were cultured in DMEM supplemented with 10% Fetal bovine serum (FBS) and penicillin/streptomycin (100 U/ml and 100 mg/ml), at 37 °C in a 5% CO_2 environment. Cells were passaged upon reaching confluence.

For cells cultured on hydrogels, cells were seeded on hydrogel disks at 1 million cells/ml concentration, and then incubated for 45min in culture medium at 37 °C, 5% CO_2.

Cell viability was assessed with a Live/Dead viability assay (Invitrogen) and laser scanning confocal microscopy (Zeiss LSM710). Prior to imaging, gels were incubated in PBS containing 4 mM Calcein AM (λ_{em} 515 nm, Invitrogen) to stain viable cells. The number of bound cells per area, on each TGT construct, was determined by manually counting the cells using the Image J (http://rsb.info.nih.gov/ij/) cell count plug in.

Cell area was assessed with ImageJ (http://rsb.info.nih.gov/ij/) software, where the threshold of the images was manually set to 95% of the pixel intensity. The cells were selected with the Wand Function and the area was calculated using built-in area calculator.

4. Focal adhesion imaging.

Focal adhesions were visualized from immunofluorescence images of vinculin at the basal plane. Cells were fixed in 4% formaldehyde in PBS, permeabilized in 0.1% Triton X-100 and washed in PBS. Cells were blocked with blocking buffer (1w/v% BSA in PBS) for 1 hour at 37°C. Next, cells were incubated with anti-vinculin mouse monoclonal primary antibody in 1:150 dilution in blocking buffer (Sigma Aldrich Clone V9131) for 45 minutes at room temperature, washed with PBS, and then incubated with secondary antibody 1:500 dilution in blocking buffer (AlexaFluor 647 anti-mouse (goat 1GG); Invitrogen A21236). The focal adhesions at the basal plane were then imaged, using laser scanning confocal microscopy (model LSM 710; Carl Zeiss MicroImaging).

RESULTS

1.Covalent TGT attachment on hydrogel substrates

TGTs with tension tolerances of T_{tol} of 12pN, 33pN, and 54pN were coupled to substrates at similar densities, regardless of the substrate modulus. These T_{tol} values are below the rupture force of individual integrin-RGD bonds [23]. Tuning the concentration of PEGDA in the pre-polymer solution altered the crosslinking density and the elastic modulus of the resulting hydrogels. Photopolymerized PEGDA solutions of 7 and 10 wt% yielded substrates with moduli of 13.1 ± 4.3 and 22.0 ± 2.1 kPa, respectively (Fig. 1A,B). Despite differences in cross-linking density, fluorescence analysis of the Cy3 reporter confirmed that the RGD density was similar on all hydrogels ($p<0.05$, N=3). The uniform fluorescence also indicated homogeneous tether coverage (Fig. S1).

2. Cell attachment depends on both substrate stiffness and TGT tension tolerance

Cell attachment was assessed for all combinations of gel stiffness and tension tolerance (T_{tol}). These DNA tethers differ in the position of force application along the dsDNA backbone, but have the same thermodynamic stability, length, and sequence (Fig. 1C). Due to the physics of the single TGT rupture, in which the self-limiting tension (tension tolerance, T_{tol}) is a determined, constant value, bond failure is independent of the gel network structure (i.e. mesh size).

After incubating cells with TGT-modified hydrogels for 45 min, we quantified cells remaining on the substrates (cell count), and observed whether they ruptured tethers (Fig. 2). Two different mechanisms controlled cell attachment (cell counts), one being mechanical and the other biochemical. The mechanical mechanism involved TGT rupture, such that the cell count decreased with increased tether tear off. This mechanism was apparent from the dark patches (shadows) on substrates where tether tear-off removed Cy3 from the substrate. Cells often endocytosed the tethers and appeared red (Fig. S2). In the second, biochemically controlled mechanism, extensive tear off was not observed, but fewer cells remained attached. Tension stabilizes integrin bonds. Under conditions where the integrin-RGD bond tension was insufficient to stabilize focal

contacts, fewer cells remained attached, and there was no obvious TGT tear off.

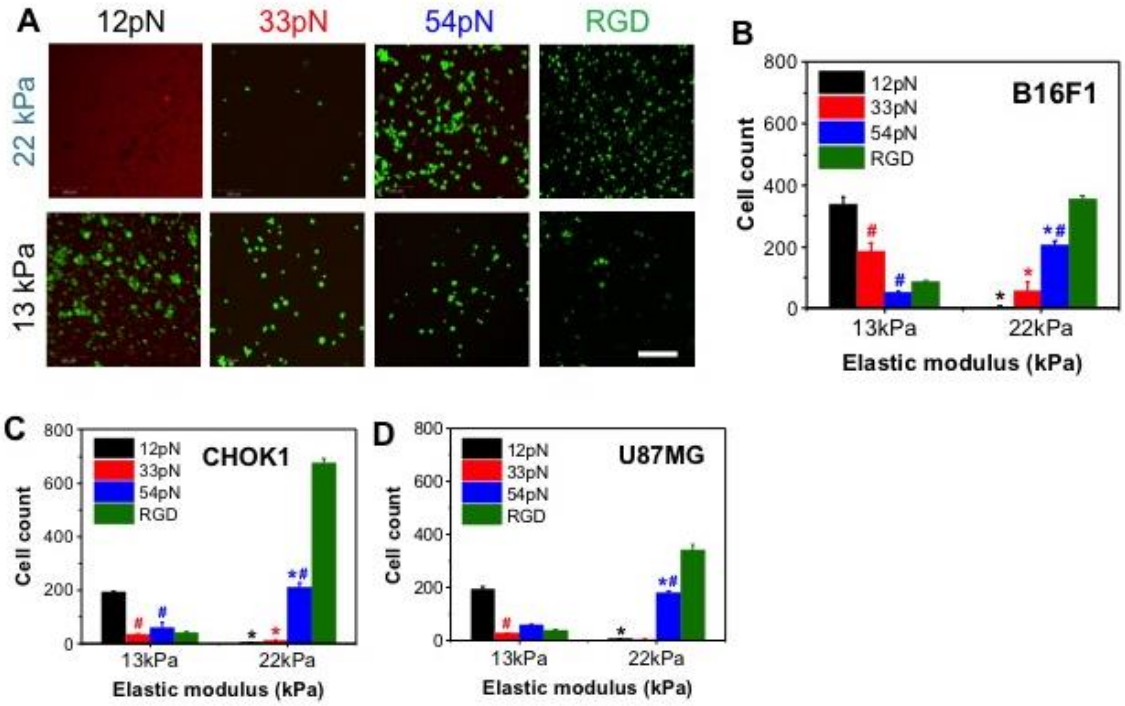

Figure 2. (A) Confocal images of adherent melanoma cells (B16F1) on compliant substrates with different elastic moduli and tension tolerance. Red designates Cy3 from the TGT and green indicates Calcein A cell staining (Live/Dead assay®). (B) Cell count as a function stiffness and tension for B16F1, (C) CHOK1 and (D) U87MG cells. Scale bar is 200 um. *p<0.05 compares cell counts on substrates with different stiffness and #p<0.05 compares different tether rupture forces (within same substrate stiffness).

Figure 2A shows images of cells and substrates after B16F1 cells were incubated with the substrates for 45 min. On the more rigid 22kPa hydrogels, the attached cell density increased with the tension tolerance T_{tol} of the tether. No cells remained on substrates with 12pN TGTs, and there were numerous shadows on the substrate, indicative of extensive tether rupture (Fig. 2A, top left). The detection of Cy3 fluorescence on cells washed off the substrates (Fig. S2) was consistent with tether tear off and endocytosis. On 33pN tethers (22kPa modulus), a few cells attached, and there was evidence of tether tear off. Numerous cells attached and TGT tear-off in the Cy3 images (Fig. S2C). These trends, and the lack of tear off at T_{tol} > 34pN agreed with reported cell adhesion on TGT-coated glass [22].

Surprisingly, on the softer hydrogels (13kPa), cell counts exhibited the opposite trend; namely, cells adhered to all substrates, regardless of the tension tolerance, but the highest cell counts were on 12pN TGT-coated gels (Fig. 2B-D).

Images of Cy3 (561 nm) coverage on the substrates exhibited few detectable dark patches (Fig. S2C), and indicated that the low cell counts on 54pN TGTs were not due to TGT tear off. Tests with CHOK1 and U87MG cells were qualitatively similar, although the absolute cell densities differed quantitatively ($p<0.05$, N=3) (Fig. 2C-D, Fig. S3).

To confirm that the inverse relationship between cell counts and T_{tol} on the softer gels was due to coupling between substrate rigidity and integrin bond tension, and not to lower ligand densities, we tested cell attachment and spreading with control, RGD-modified hydrogels. With 13kPa and 22kPa gels modified with the non-rupturable PEG-RGD ligand, more cells attached to the stiffer gel. This was as expected, based on reported positive feedback between integrin tension and the activation of a high affinity integrin state and cell spreading (Fig. 2) [14]. The control measurements also confirmed that the low cell counts on soft, TGT-modified gels were not due to differences in ligand accessibility (Figs. 1A-D,S3).

3. Substrate stiffness regulates cell attachment and spreading on intact TGTs.

Both membrane and actomyosin-generated tension appear to influence integrin-mediated cell adhesion and spreading, but at different, distinct phases [5, 7, 24]. To test whether the inability of cells to spread on and rupture 12pN TGTs on soft gels was due to arrested transitions to the spreading P1 and contractile P2 phases, we tested whether nascent focal adhesions formed on compliant, low T_{tol}, substrates, by imaging vinculin at the basal plane. Vinculin—an actin binding protein—is a common marker for FAs [25]. Fig. 3A shows overlaid bright field and vinculin immunofluorescence images at the basal planes of cells on the different substrates. Vinculin staining was observed with cells on 54 pN tethers, regardless of the substrate stiffness (Figs. 3A). By contrast, although more cells remained attached to 12pN tethers on soft gels (than on 54pN tethers), cells remained round and there was no apparent vinculin staining (Fig. 3A). The latter behavior was

consistent with inability of cells to transition to the spreading P1 phase. Generally, cells spread more effectively on higher T_{tol} substrates, regardless of the gel stiffness (Table S1). However, the lack of spreading on 12pN substrates suggested that the spreading transition threshold lies between 12pN and 33pN, which is slightly lower than the 37pN estimated from membrane tension measurements [5].

On 33pN tethers, integrin adhesions recruited vinculin on the stiffer 22kPa gels, but not on the soft gels. Thus, substrate rigidity reduced the tension cells exerted on individual 33pN tethers, preventing both tether tear off and vinculin recruitment observed on 22kPa gels.

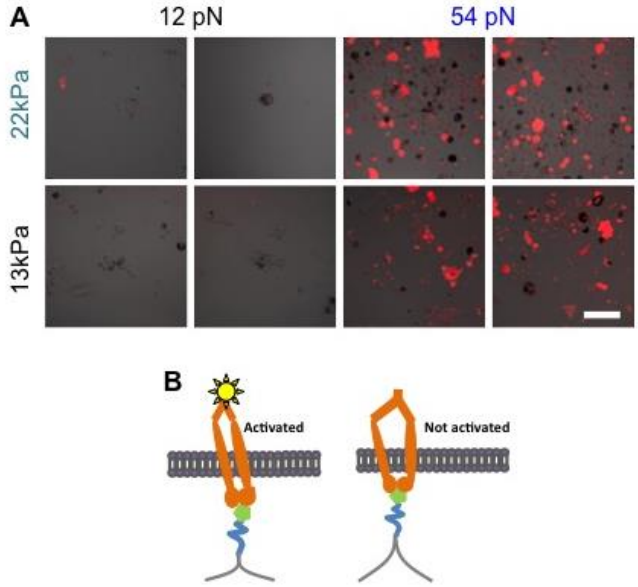

Figure 3. (A) Confocal immunoflourescence images of vinculin at the basal plane of B16F1 cells on substrates of different stiffness and tension tolerance. Scale bar is 100 um. (B) Model of integrin activation (leading to vinculin recruitment) upon RGD binding.

DISCUSSION

These findings revealed nanoscale coupling between substrate stiffness and force thresholds underlying decision-making in cell adhesion and spreading. Notably, on rigid, glass substrates, cells ruptured 12pN tethers and detached; consequently, the unexpectedly greater cell attachment and lack of spreading on 12pN TGTs on soft gels exposed coupling between bond tension, substrate mechanics, and cell biochemistry.

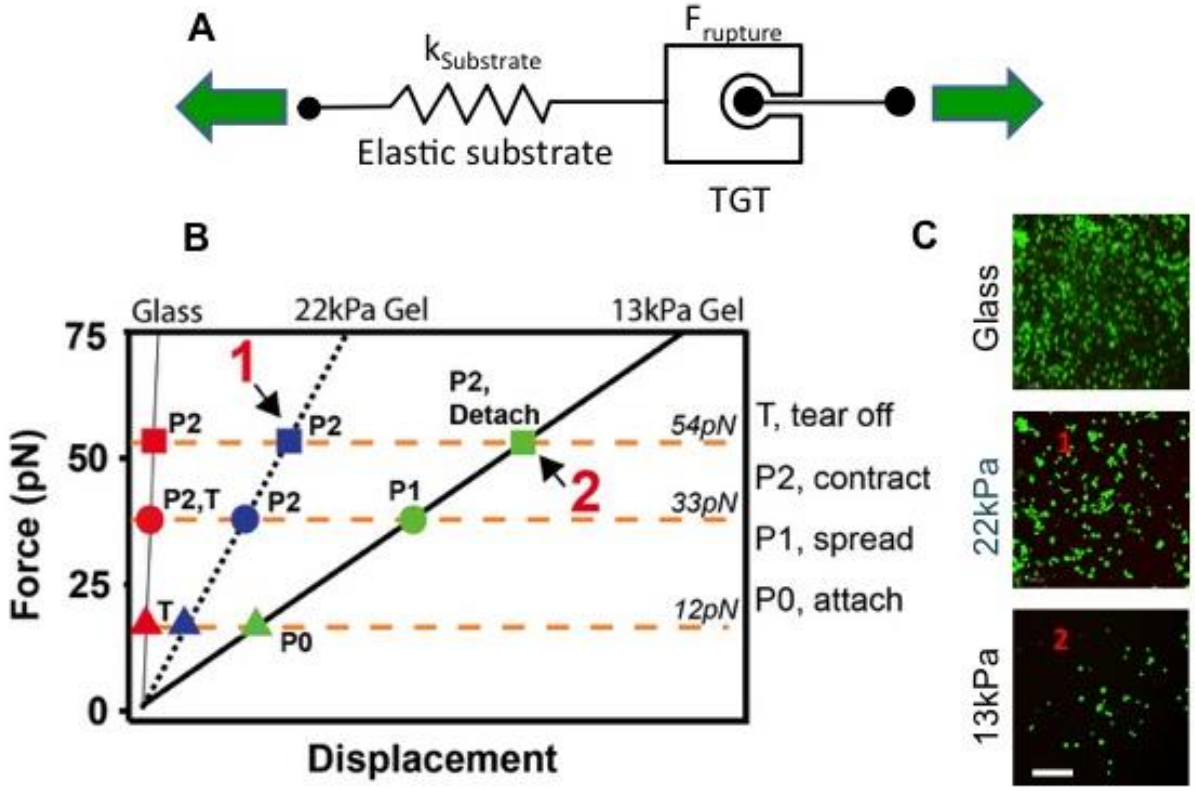

Figure 4. (A) Proposed model of a cell attached to a tether-hydrogel substrate. System deformations resulting in failure are uniquely defined by the combination of gel stiffness and TGT tear off force. (B) Force versus total displacement determined by the spring-lock system and resulting observed cell behavior. The slope of the force vs displacement curve is determined by the substrate stiffness. The force on individual bonds increases to the T_{tol} of the tether, indicated by the horizontal gold, dashed lines at 12, 33, and 54pN. Above T_{tol}, the tethers fail. The substrate moduli determine the total system displacement (deformation) at the point of failure. Red, blue, and green correspond to different substrate moduli, and triangles, circles, and squares correspond to different T_{tol}. The different labels correspond to observed cell behavior observed for the different combinations of T_{tol} and substrate modulus. (C) B16F1 cell attachment to different substrates modified with 54 pN TGTs. Conditions indicated by numbers 1 and 2 are indicated in the graph in panel *B*. Scale bar 200 um.

Rigidity-dependent cell attachment and spreading are largely attributed to positive feed back between contractile forces exerted on integrins and substrate compliance [4, 15, 26]. Increasing force on focal contacts is presumed to trigger biochemical changes underlying transitions in cell spreading and adhesion maturation, above threshold forces associated with force-activated changes in protein conformations and interactions [5, 7, 27, 28]. An open question has been whether cellular decision-making depends solely on forces exerted by cells, and whether those cellular forces depend on the substrate compliance.

To account for our findings, we proposed a mechano-chemical model that describes the system as a spring in series with a bolt, where the elastic substrate and TGTs are the spring and bolts, respectively (Fig. 4A). As the cell initially exerts force on substrates, through actin flow, membrane tension, or contractility, for example, it deforms the system (substrate and cell membrane) until the elastic restoring force - defined by Hookes law ($F_{deform} = k_{sub} x$) – equals T_{tol}. If the force on the TGTs exceeds T_{tol}, then the cell detaches, leaving a dark footprint where the Cy3 dye is removed. In our model, the substrate modulus determines the slope of the force-displacement curves (Fig. 4B), and the maximum displacement x_{max} at T_{tol}. Potential coupling between bond tension (T_{tol}), substrate compliance (deformations), and integrin biochemistry could shift cell attachment and spreading behavior, in unexpected ways. The surprising difference in the rigidity-dependent cell counts on 12pN versus 54pN tethers can be explained in the context of this model (Fig. 4A,B), and the corresponding decision tree is illustrated in Fig. 5. On soft gels, smaller deformations on 12pN TGTs, relative to 54pN TGTs (Fig. 4B), would activate integrin-RGD ligation and clustering, resulting in 'stable' cell attachment. However, the capped forces are insufficient to activate the membrane-spreading phase P1, so that cells remain round (P0). The model also explains cell attachment to the stiff 12pN T_{tol} gels. On stiff gels, displacement fluctuations would generate greater force fluctuations and more frequent tether tear off (dark patches) (Fig. 2A). Small displacements may also instruct further increases in bond tension, and subsequent tether tear off.

On 33pN tethers, the substrate stiffness appeared to alter the force threshold at which cells transitioned to the contractile P2 phase of cell spreading, as marked by vinculin

recruitment. Cells spread on both soft and rigid 33pN T_{tol} substrates, but only recruited vinculin to FAs on the rigid gels, despite the identical tether T_{tol}. In the context of our model, smaller deformations on the stiffer gels are postulated to instruct increased cell contractions and vinculin accumulation, and hence the transition to P2.

With 54pN T_{tol} tethers, cells transitioned to P2 and recruited vinculin to FAs, but the substrate stiffness influenced whether cells attached stably and spread, or detached without TGT rupture. The lower cell density on softer ECM (13kPa) is consistent with the formation of weaker integrin bonds, more extensive β1 integrin internalization in cells on soft ECM [9], and forces below levels needed to stabilize integrin bonds [29].

These analyses and the 'decision-tree' in Fig. 5 account for the inverse dependence of cell counts on T_{tol} on soft versus rigid gels. The inability of large deformations to activate increases in bond tension on soft, low T_{tol} (12 pN) substrates prevented spreading and tether tear off, resulting in higher densities of attached, rounded cells.
At higher T_{tol}, cell attachment decreased due to tear off (33pN) and to the negative effects of stiffness on integrin affinity [9]. On rigid substrates, small substrate deformations triggered increased contractility, so that tethers failed catastrophically, and cells detached, leaving footprints (Fig. S2). Thus, cell density increased with increasing T_{tol}.

Our findings support the postulate that force thresholds instruct cell spreading, contraction, and FA maturation (Fig. 5), but also suggest that the substrate stiffness alters the force thresholds. Low or undetectable 12pN TGT tear-off on soft gels indicated that forces exerted by cells on surviving tethers were ≤12pN, and insufficient to activate spreading (P0→P1). Cells spread on 33pN tethers on both soft and stiff hydrogels. The greater vinculin recruitment—associated with the putative transition to the contractile phase—on stiff gels suggested that the force threshold to activate cell contractions is ~33pN. At higher T_{tol}, forces up to 54pN supported vinculin accumulation at focal adhesions on both soft and rigid gels, although more cells subsequently detached from the softer ECM. In the latter cases, the lack of tether tear off suggested that the force on the

nascent focal contacts was below 54pN. Interestingly, a recent tension sensor reported forces exceeding 100pN in mature FAs [30].

Measured spread cell areas (Table S1) agreed with another report of spread cell areas on different tension tolerant substrates [31]. Cell spreading depends on both bond density and bond tension, and tether failure reduces bond density. Thus, reported spreading differences were likely due to combined effects of the bond tension capped by TGTs and surviving integrin bonds. Our findings indicated force thresholds for postulated spreading transitions, and also suggested that ECM stiffness alters those thresholds. This was apparent from the cell densities reported in this study that revealed coordinated influences of substrate deformations and receptor biochemistry (bond tension) on cell attachment stability and spreading transitions.

The role of nanoscale deformations in cellular decision-making, as suggested by our model, is supported by the quantized displacements of arrayed micropillars, by attached cells. The quantized displacements appear to be due to tropomyosin-dependent, rigidity-sensing units that operate during the contractile spreading phase [32]. Studies using TGTs anchored to individual, end-grafted polymer chains of different extensibility suggested that this may not apply for individual receptor displacements.

However, a likely explanation for the different conclusions is that collective deformations over larger membrane (and cytoskeletal) regions than individual ligands may be necessary for sensing ECM rigidity. Indeed, the spring constant for bulk substrate deformations k_{sub} is related to the Young's modulus (E) through the cross-sectional area (A) and the rest length L_0 of the spring: $k_{sub} = E\ A\ /\ L_0$. The minimum integrin density required to support cell spreading also implies rigidity sensing through larger molecular assemblies [8, 33]. Our results do not resolve this issue, but we note the differences in the experimental platforms used.

Our proposed phenomenological model (Fig. 4A,B) also captures differences in strain rates, because larger deformations require longer times [34]. Strain dynamics are

biochemically relevant because force sensing involves dynamic changes in biomolecular reactivity and protein conformations, as in the case of talin, as well as periodic contractions near the edges of spreading cells [32, 35-37]. Similarly, integrin endocytosis on soft substrates involves dynamic biochemical processes as well as membrane deformations [9]. The deformation rates relative to these processes could also instruct cell behavior. In summary, these autonomously-force-limiting TGTs exposed coupling between substrate mechanics and forces regulating cell attachment and spreading. We explain these results with a mechanical model in which coupled substrate deformations and bond rupture alter the force thresholds that regulate cell attachment and spreading on compliant matrices.

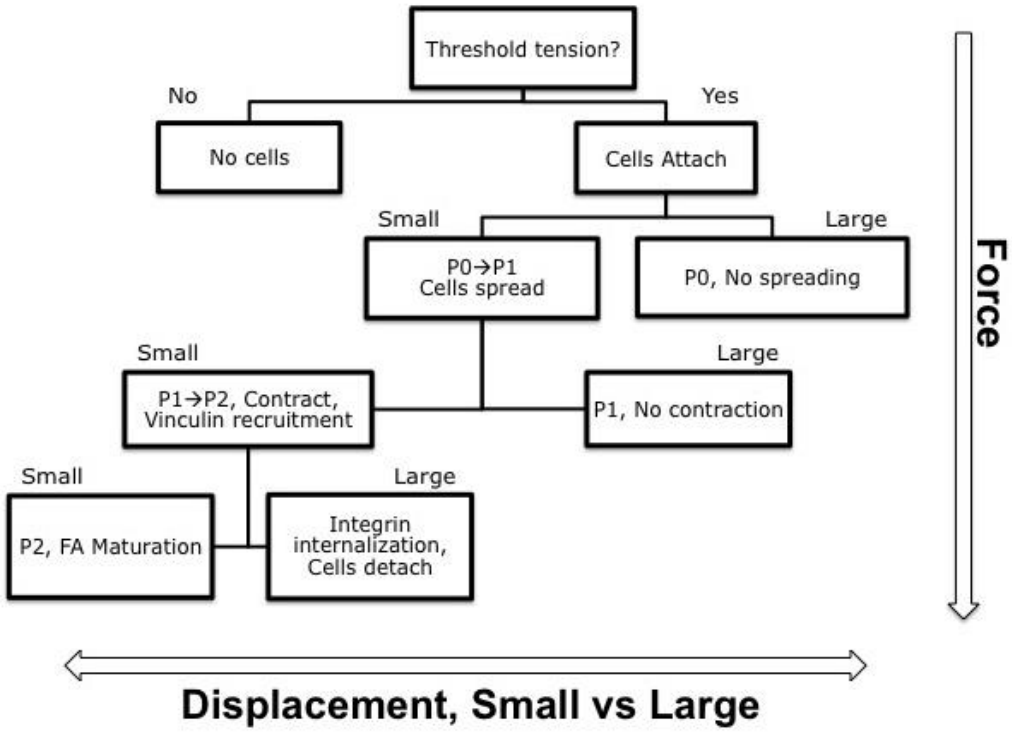

Figure 5. Force and displacement instruct cellular decision-making during cell attachment, spreading and focal adhesion maturation.

SUPPLEMENTARY FIGURES

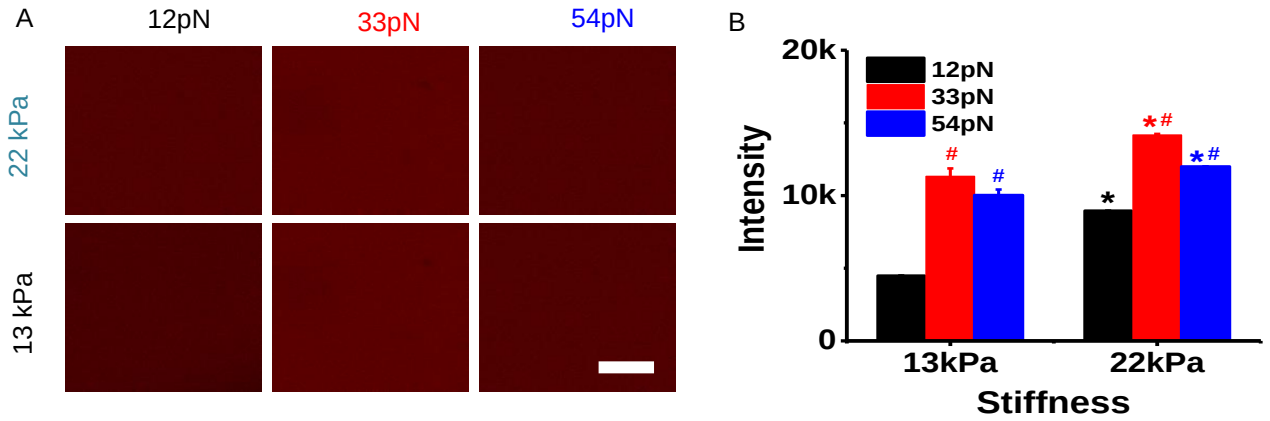

Figure S1. (A) Fluorescence image of Cy3-labeled TGT constructs with different combinations of tension tolerance (12 - 54 pN) and hydrogel stiffness (13 - 22 kPa) after washing. (B) Fluorescence intensity is higher in more crosslinked networks due to restricted bond rotation by steric hindrance. TGT density was calibrated for all substrates and adjusted to tether reactivity during PEGDA photopolymerization. * $p<0.05$ between different stiffness groups and #$p<0.05$ between different tether forces.

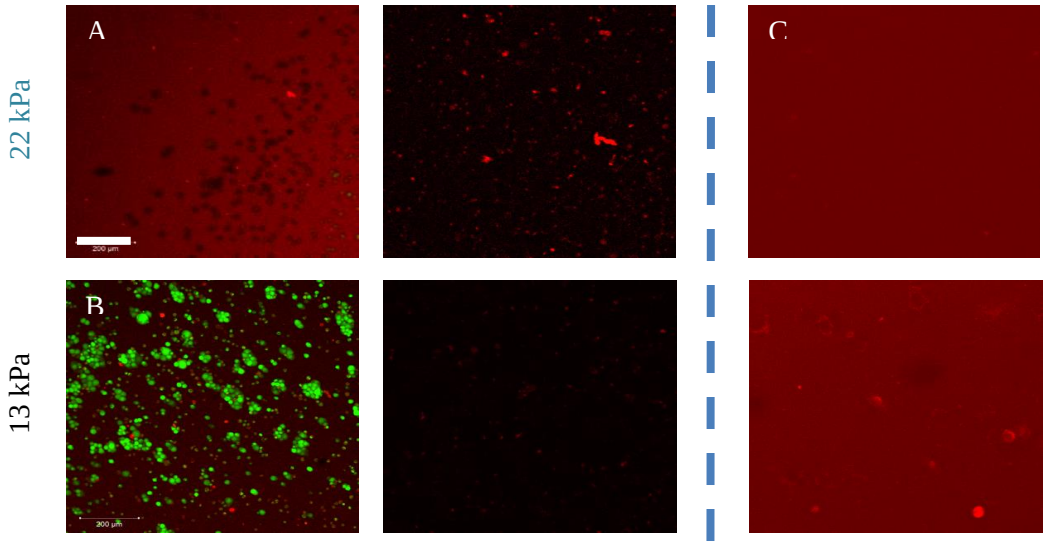

Figure S2. (A) B16F1 cells adhere or rupture 12 pN TGTs on more and less compliant surfaces respectively. (B) Confocal images of resulting washed B16F1 cells that are labelled with Cy3 from internalized ruptured RGD tethers. (C) Cy3 channel of surfaces with 54 pN TGTs and seeded B16F1 cells, where no shadows are observed.

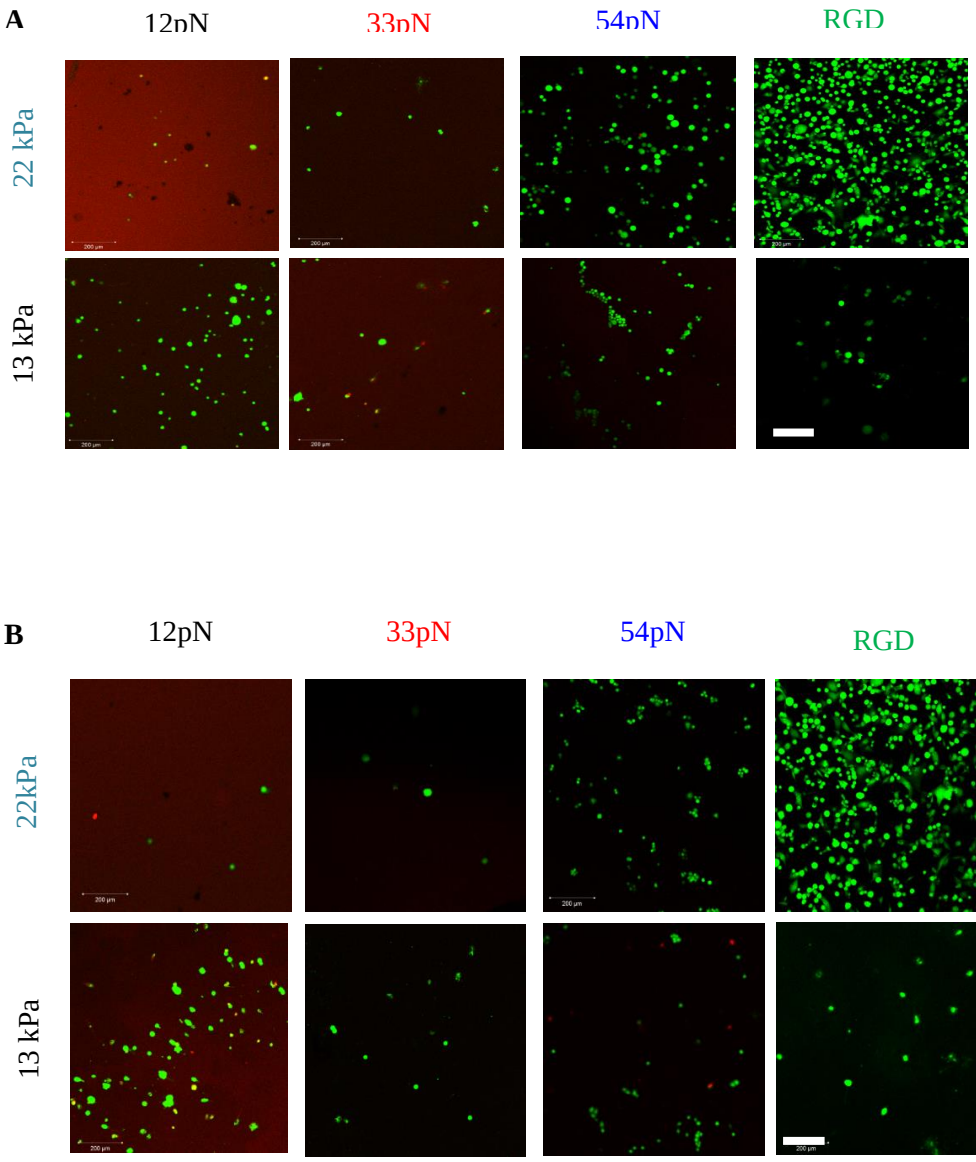

Figure S3. Confocal images of adherent (A) ovary (CHOK1) and (B) glioma cells on soft substrates of different stiffness and tension tolerance. Red designates Cy3 from TGT and green Calcein A cell staining (Live/Dead assay®). Scale bar is 200 um.

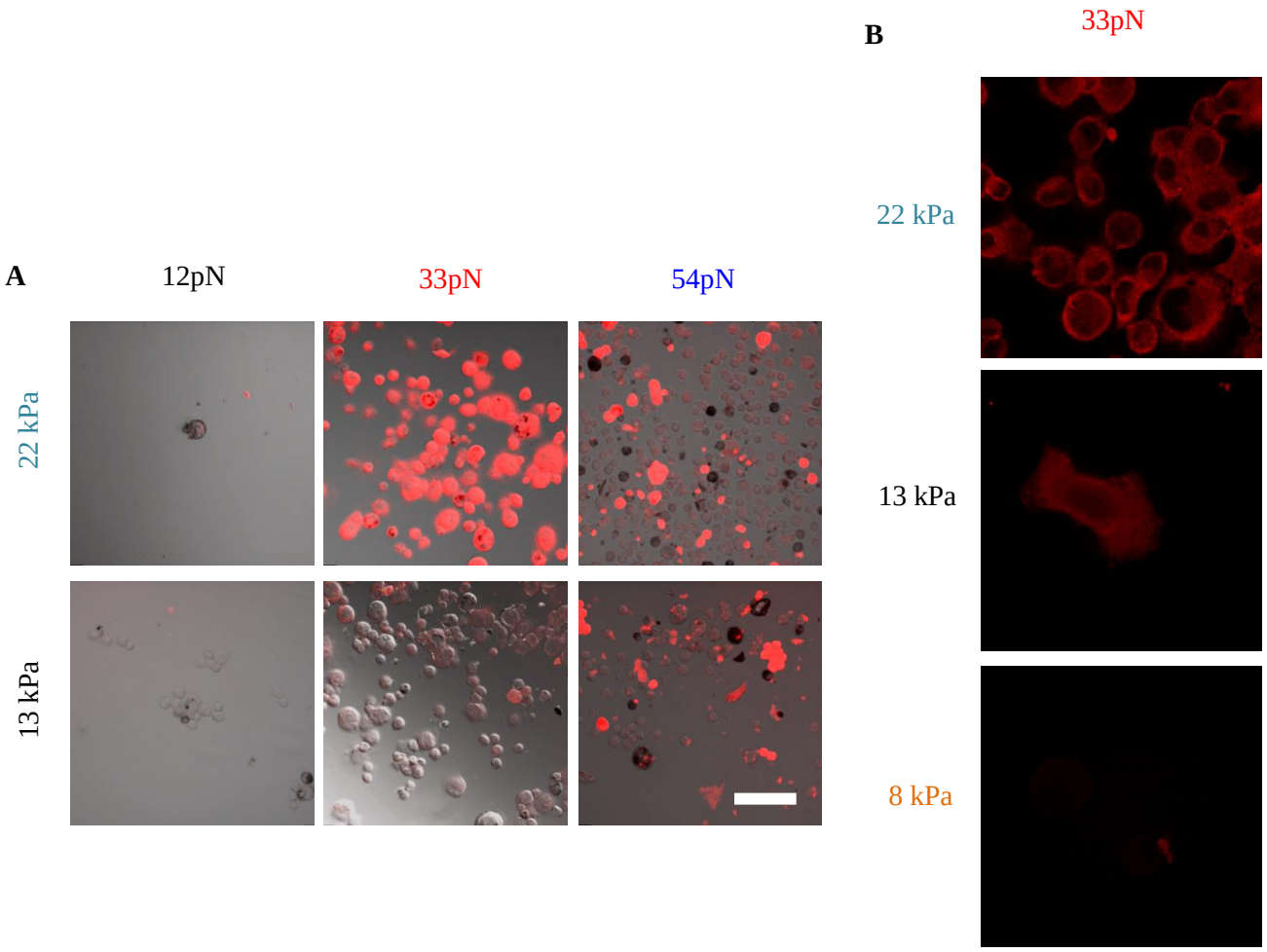

Figure S4. Vinculin staining of B16F1 cells to show the recruitment of vinculin at focal adhesion on substrates of different combinations of stiffness and tension tolerance. (A) Scale bar is 100 mm. (B) Scale bar is 50 mm.

REFERENCES

1. N. Q. Balaban, U. S. Schwarz, D. Riveline, P. Goichberg, G. Tzur, I. Sabanay, D. Mahalu, S. Safran, A. Bershadsky, L. Addadi and B. Geiger, *Nat Cell Biol*, 2001, **3**, 466-472.
2. D. Riveline, E. Zamir, N. Q. Balaban, U. S. Schwarz, T. Ishizaki, S. Narumiya, Z. Kam, B. Geiger and A. D. Bershadsky, *J Cell Biol*, 2001, **153**, 1175-1186.
3. A. D. Bershadsky, N. Q. Balaban and B. Geiger, *Annu Rev Cell Dev Biol*, 2003, **19**, 677-695.
4. B. Geiger, J. P. Spatz and A. D. Bershadsky, *Nature reviews*, 2009, **10**, 21-33.
5. N. C. Gauthier, M. A. Fardin, P. Roca-Cusachs and M. P. Sheetz, *Proc Natl Acad Sci U S A*, 2011, **108**, 14467-14472.
6. O. M. Rossier, N. Gauthier, N. Biais, W. Vonnegut, M. A. Fardin, P. Avigan, E. R. Heller, A. Mathur, S. Ghassemi, M. S. Koeckert, J. C. Hone and M. P. Sheetz, *EMBO J*, 2010, **29**, 1055-1068.
7. H. Wolfenson, T. Iskratsch and M. P. Sheetz, *Biophys J*, 2014, **107**, 2508-2514.
8. E. A. Cavalcanti-Adam, A. Micoulet, J. Blummel, J. Auernheimer, H. Kessler and J. P. Spatz, *Eur J Cell Biol*, 2006, **85**, 219-224.
9. J. Du, X. Chen, X. Liang, G. Zhang, J. Xu, L. He, Q. Zhan, X. Q. Feng, S. Chien and C. Yang, *Proc Natl Acad Sci U S A*, 2011, **108**, 9466-9471.
10. A. J. Engler, S. Sen, H. L. Sweeney and D. E. Discher, *Cell*, 2006, **126**, 677-689.
11. C. C. DuFort, M. J. Paszek and V. M. Weaver, *Nat Rev Mol Cell Biol*, 2011, **12**, 308-319.
12. P. Lu, V. M. Weaver and Z. Werb, *J Cell Biol*, 2012, **196**, 395-406.
13. D. T. Butcher, T. Alliston and V. M. Weaver, *Nat Rev Cancer*, 2009, **9**, 108-122.
14. J. C. Friedland, M. H. Lee and D. Boettiger, *Science*, 2009, **323**, 642-644.
15. U. S. Schwarz and M. L. Gardel, *J Cell Sci*, 2012, **125**, 3051-3060.
16. C. G. Galbraith, K. M. Yamada and M. P. Sheetz, *J Cell Biol*, 2002, **159**, 695-705.
17. N. Borghi, M. Sorokina, O. G. Shcherbakova, W. I. Weis, B. L. Pruitt, W. J. Nelson and A. R. Dunn, *Proc Natl Acad Sci U S A*, 2012, **109**, 12568-12573.
18. M. Morimatsu, A. H. Mekhdjian, A. S. Adhikari and A. R. Dunn, *Nano letters*, 2013, **13**, 3985-3989.

19. T. J. Kim, S. Zheng, J. Sun, I. Muhamed, J. Wu, L. Lei, X. Kong, D. E. Leckband and Y. Wang, *Curr Biol*, 2015, **25**, 218-224.
20. C. Grashoff, B. D. Hoffman, M. D. Brenner, R. Zhou, M. Parsons, M. T. Yang, M. A. McLean, S. G. Sligar, C. S. Chen, T. Ha and M. A. Schwartz, *Nature*, 2010, **466**, 263-266.
21. D. R. Stabley, C. Jurchenko, S. S. Marshall and K. S. Salaita, *Nat Methods*, 2012, **9**, 64-67.
22. X. Wang and T. Ha, *Science*, 2013, **340**, 991-994.
23. C. M. Franz, A. Taubenberger, P. H. Puech and D. J. Muller, *Sci STKE*, 2007, **2007**, pl5.
24. P. Roca-Cusachs, N. C. Gauthier, A. Del Rio and M. P. Sheetz, *Proc Natl Acad Sci U S A*, 2009, **106**, 16245-16250.
25. R. M. Ezzell, W. H. Goldmann, N. Wang, N. Parasharama and D. E. Ingber, *Exp Cell Res*, 1997, **231**, 14-26.
26. B. Geiger and K. M. Yamada, *Cold Spring Harb Perspect Biol*, 2011, **3**.
27. V. Vogel and M. Sheetz, *Nat Rev Mol Cell Biol*, 2006, **7**, 265-275.
28. J. Takagi and T. A. Springer, *Immunol Rev*, 2002, **186**, 141-163.
29. C. K. Choi, M. Vicente-Manzanares, J. Zareno, L. A. Whitmore, A. Mogilner and A. R. Horwitz, *Nat Cell Biol*, 2008, **10**, 1039-1050.
30. K. Galior, Y. Liu, K. Yehl, S. Vivek and K. Salaita, *Nano letters*, 2015, DOI: 10.1021/acs.nanolett.5b03888.
31. F. Chowdhury, I. T. Li, B. J. Leslie, S. Doganay, R. Singh, X. Wang, J. Seong, S. H. Lee, S. Park, N. Wang and T. Ha, *Integrative biology : quantitative biosciences from nano to macro*, 2015, **7**, 1265-1271.
32. H. Wolfenson, G. Meacci, S. Liu, M. R. Stachowiak, T. Iskratsch, S. Ghassemi, P. Roca-Cusachs, B. O'Shaughnessy, J. Hone and M. P. Sheetz, *Nat Cell Biol*, 2015, DOI: 10.1038/ncb3277.
33. E. A. Cavalcanti-Adam, T. Volberg, A. Micoulet, H. Kessler, B. Geiger and J. P. Spatz, *Biophys J*, 2007, **92**, 2964-2974.
34. A. Elosegui-Artola, E. Bazellieres, M. D. Allen, I. Andreu, R. Oria, R. Sunyer, J. J. Gomm, J. F. Marshall, J. L. Jones, X. Trepat and P. Roca-Cusachs, *Nat Mater*, 2014, **13**, 631-637.

35. A. del Rio, R. Perez-Jimenez, R. Liu, P. Roca-Cusachs, J. M. Fernandez and M. P. Sheetz, *Science*, 2009, **323**, 638-641.
36. S. E. Lee, R. D. Kamm and M. R. Mofrad, *J Biomech*, 2007, **40**, 2096-2106.
37. S. Ghassemi, G. Meacci, S. Liu, A. A. Gondarenko, A. Mathur, P. Roca-Cusachs, M. P. Sheetz and J. Hone, *Proc Natl Acad Sci U S A*, 2012, **109**, 5328-5333.